

TSUNAMI GENERATION BY 3D DEFORMABLE GRANULAR LANDSLIDES

Fahad Mohammed¹, Brian C. McFall¹, and Hermann M. Fritz¹

¹ School of Civil and Environmental Engineering, Georgia Institute of Technology, 210 Technology Circle, Savannah, GA 31407, USA.
fahd@gatech.edu, bmcfall3@gatech.edu, fritz@gatech.edu

Abstract: Landslide generated tsunamis are particularly hazardous in enclosed water bodies. Topographical and bathymetric features can either dissipate or enhance the generated waves leading to potentially extensive damages. To study the effect of such features landslide generated tsunami experiments were conducted in physical scale models representing fjords, headlands and farfield hill slopes. A pneumatic landslide tsunami generator deploys unconfined deformable granular landslides on a hill slope which impact the water surface and thereby generate tsunami waves. The instrumentation setup includes multiple cameras, particle image velocimetry, acoustic transducers and an array of wave gauges. Landslide measurements are made to characterize the source properties. The wave profile recordings with and without the topographic features provide insights into their effects on the tsunami wave characteristics. A fjord setup traps and distributes the wave energy along the fjord slopes in the channel, while a headland captures only part of the energy and radiates the rest into the open basin.

INTRODUCTION

Landslide generated tsunamis can occur in confined water bodies, at islands, continental shelves and coasts where the wave can travel both in offshore and along the shore directions. Tsunamis generated by landslides can have locally extremely high amplitudes and runup and can be particularly devastating in the near field regions. Major tsunamis caused by landslides were recorded by the ancient Storegga slides (Bondevik et al., 2005), at Grand Banks, Newfoundland in 1929 (Fine et al.,

2005), Lituya Bay, Alaska in 1958 (Miller, 1960; Fritz et al., 2001, 2009; Weiss et al., 2009), Vajont dam in Italy in 1963 (Müller, 1964), 1998 Papua New Guinea (Synolakis et al., 2002; Bardet et al., 2003), Stromboli (Tinti et al., 2005, 2006) and Java (Fritz et al., 2007). The generated waves can cause damage mainly due to large local runup along the coastline and overtopping of dams and reservoirs. Presence of bathymetric and topographical features can either amplify or reduce the generated waves, potentially increasing the damage associated with landslide tsunamis. The largest recorded tsunami runup was observed in Lituya Bay Alaska in 1958. The maximum runup of 524 m was recorded on the opposing headland in the prolongation of the landslide motion as shown in Fig. 1.

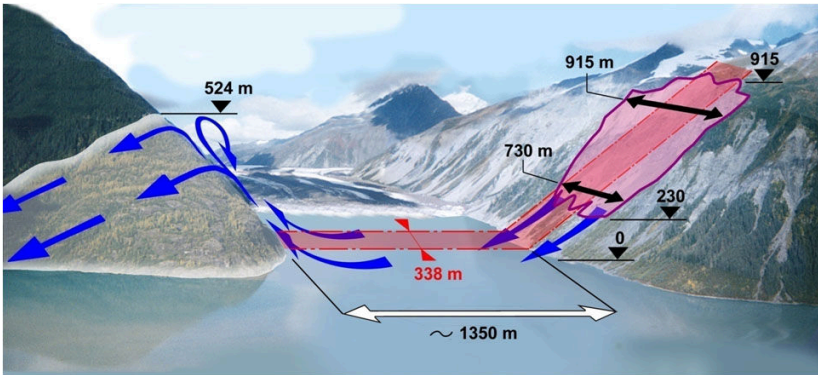


Fig. 1. The 1958 Lituya Bay tsunami event in Alaska showing the maximum recorded tsunami runup of 524 m in the direction of landslide prolongation inside Gilbert Inlet (Fritz et al., 2001).

The information from landslide tsunami events is mostly limited to runup trimlines, farfield tide gauge recordings and submarine landslide deposits where mapped. Hence, landslide generated tsunamis are physically modeled to study the wave generation, propagation and runup in setup scenarios representing fjords, headlands and regional coasts. Historically the majority of the experiments have focused on two dimensional tsunami waves generated by landslides. These experiments were performed by using either solid blocks sliding on an incline to simulate landslide tsunamis (Heinrich, 1992; Watts, 2000; Walder et al., 2003; Grilli and Watts, 2005) or granular landslides (Fritz et al., 2003 and 2004). Waves generated by three dimensional solid block landslides on flat bottoms, sloping beaches and conical islands were studied by Liu et al. (2005), Panizzo et al. (2005), Enet and Grilli (2005 and 2007); DiRisio et al. (2009). Tsunami generation by three dimensional deformable granular landslides is studied by Mohammed and Fritz (2010) and herein extended to physical models of fjords, headlands and runup on regional coastlines.

PHYSICAL MODEL

The physical model experiments based on the generalized Froude-similarity were performed at the Network for Earthquake Engineering Simulation (NEES) Tsunami

Wave Basin at the O. H. Hinsdale Wave Research Laboratory at Oregon State University in Corvallis. Three-dimensional models of fjords, headlands and offshore hill slope were constructed in the wave basin with a slope $\alpha=27.1^\circ$. Three-dimensional granular landslides were deployed on a hill slope by means of a pneumatic landslide tsunami generator (LTG) with the ability to control the landslide kinematics and shape. The landslide tsunami generator is capable of simulating landslides initiating both above and below the water surface. The landslides are modeled with naturally rounded river gravel with $d_{50}=13.7\text{mm}$, grain density $\rho_g=2.60\text{t/m}^3$, bulk slide density $\rho_s=1.76\text{t/m}^3$, porosity 0.31, internal friction angle $\varphi=41^\circ$ and basal friction angle $\delta=23^\circ$. The landslide masses of 1350 kg and 675 kg were considered for the experimental tests.

State-of-the-art instrumentation is deployed in the wave basin to measure the characteristics of the granular landslide motion and generated tsunami waves. The landslide shape and velocity on the hill slope are measured from the image sequences recorded by multiple above and underwater cameras. A high resolution particle image velocimetry camera setup determines the landslide surface velocity distribution during the subaerial motion. A multi-transducer acoustic array (MTA) measures the submarine slide deposit shape, volume and runout distance. The offshore propagating wave surface profiles are measured by numerous resistance wave gauges deployed throughout the tsunami wave basin. A series of runup wave gauges record the tsunami runup on the landslide hill slope and the offshore slopes composing the fjord, headland or distant regional coastlines. The wave propagation and runup characteristics are determined from the wave profiles recorded by the wave gauge array. The wave gauge locations for the fjord setup are shown in Fig. 2.

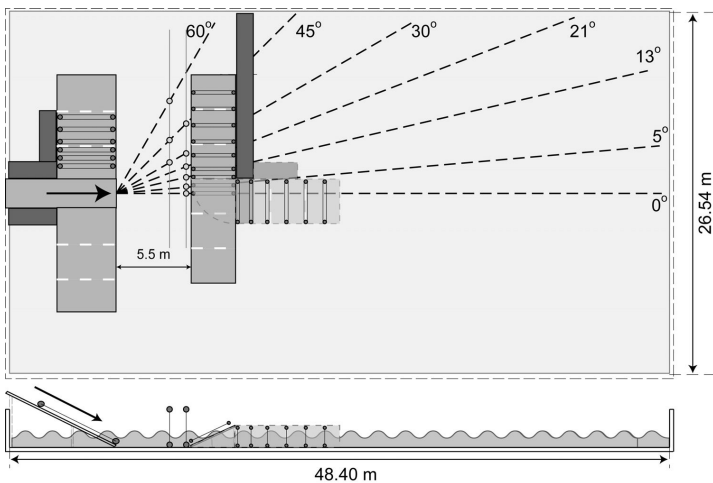


Fig. 2. Experimental setups superimposed for the two case scenarios of landslide generated tsunamis in a fjord with a straight opposing coastline and a headland with a 90° bend facing the landslide axis.

A total of 144 experimental trials were conducted by varying the control parameters of the landslide motion and the water depths in the tsunami wave basin. The variation of initial landslide volume and pneumatic accelerations provided a range of experimental conditions concerning the landslide motion at impact. Two different landslide volumes of 0.378 m^3 and 0.756 m^3 are accelerated by four initial pneumatic accelerations. The varying landslide volumes and initial accelerations result in various scenarios of tsunami generation by granular landslides. The varying water depths enabled to study the wave generation, propagation and runup spanning across the shallow, intermediate and deep water depth wave regimes. Landslides were deployed at water depths of 0.3, 0.6, 0.9 and 1.2 m in the wave basin.

LANDSLIDE SOURCE DESCRIPTION

The granular landslide material is initially contained in the landslide tsunami generator (LTG) box and accelerated by means of four pneumatic pistons. At approximately the peak box velocity, the landslide material is released from the box and transforms to gravity driven granular landslide motion on the hill slope. The landslide moves down the hill slope, impacts on the water body and generates the tsunami waves. The landslide motion is described by a coordinate system following the hill slope. The x_s direction of motion is along the hill slope, y_s is in the lateral direction and z_s is in the orthogonal direction to the hill slope. The origin for this coordinate sub-system is at the initial rest position of the landslide front.

The landslide shape is measured from the above water side camera imagery. The thickness is obtained as functions of propagation distance on the hill slope and time, $s(x_s, t)$. The thickness profiles for landslide volume $V_s = 0.756 \text{ m}^3$, landslide release velocity $v_b = 3.8 \text{ m/s}$, and the impact location at $x_s = 3.36 \text{ m}$ are shown in Fig.3(a). The granular landslides have typical longitudinal axis profiles characterized by a sharp front leading to a peak slide thickness and a gradual decay towards the tail of the landslide. The slope of the front and the spread of the slide depend on the initial landslide volume and the release velocity from the box. The maximum slide thickness is obtained from the measured slide shape along the hill slope. The maximum thickness and width along the hill slope are shown in Fig. 3(b).

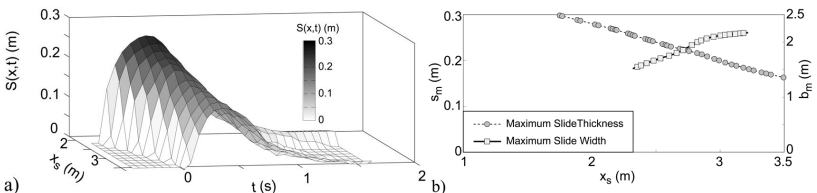


Fig. 3. Landslide shape for $V_s = 0.756 \text{ m}^3$ and $v_b = 3.8 \text{ m/s}$: (a) thickness profile $s(x_s, t)$ and (b) maximum slide thickness s_m and width b_m .

Subsequent to the landslide collapse onto the plane hill slope, the downward motion of the landslide is accompanied by an unconfined lateral spreading. The lateral width of the landslide influences the width of the water displacement area or the crater at impact of the granular landslide on the water surface. The landslide width, thickness

and velocity at impact determine the rate of mass, momentum and energy flux of the landslide. As a consequence, they influence the radial spreading of the generated waves and the decay rates of the wave amplitudes. The width is determined from the image sequences recorded by the PIV camera. A combination of time stacking, image filtering and image averaging is applied to segment the image and extract the width of the landslide. The width is obtained as functions of space and time $b(x_s, t)$ and the envelop of width b_m along the hill slope (Fig. 3b).

The landslide front velocity is measured from the combination of above water side and PIV cameras. During the initial phase of the landslide motion, the landslide front velocity corresponds to the slide box velocity until the landslide material departs from the slide box. After the release, the gravity driven landslide motion on the hill slope is determined by landslide front measurements from the camera images. The front velocity for landslide volume $V_s = 0.756 \text{ m}^3$, slide release velocity $v_b = 3.8 \text{ m/s}$ is shown in Fig. 4, with the slide impact location at $x_s = 3.36 \text{ m}$.

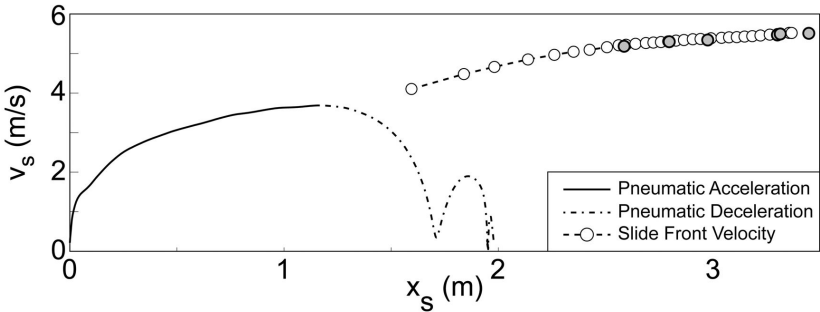


Fig. 4. Slide front velocity v_s for a case with slide volume $V_s=0.756 \text{ m}^3$ and release velocity $v_b=3.8 \text{ m/s}$. Hollow circles are measured from side camera and filled circles from landslide surface PIV analysis.

The velocity distribution on the landslide surface is obtained from planar cross-correlation analysis based Particle Image Velocimetry (PIV) processing of the image sequences. The speckle-like patterns on landslide granulate surfaces are used for iterative multi-pass cross correlation analysis with decreasing window sizes from 128 by 128 down to 32 by 32 pixels (Raffel et al. 1998; Fritz et al. 2003a). The image background is masked to isolate the landslide surface from the water surface. The velocity vector distribution on the landslide surface is shown for a run with landslide volume $V_s = 0.756 \text{ m}^3$, $v_b = 3.8 \text{ m/s}$ and impact velocity $v_s = 5.5 \text{ m/s}$. The velocity distribution, U_s , is steady across the bulk of the lateral landslide width. The velocity maximum is at the landslide center where the bulk of the granular material persists. The velocity decreases from the axis towards the edge of the granular landslide. The peak velocity however increases steadily down the slope due to the buildup of momentum as driving gravity dominates restraining friction losses.

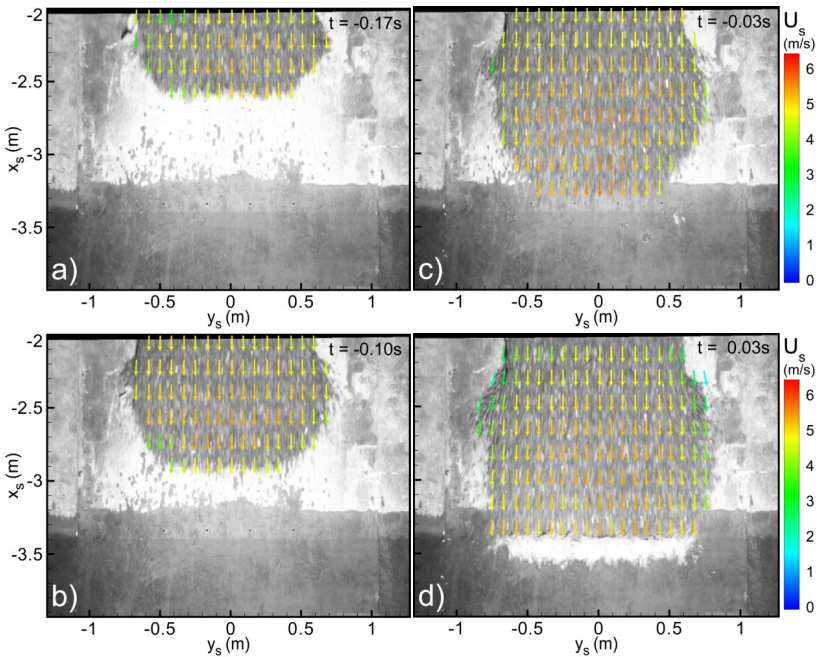


Fig. 5. Planar PIV landslide surface velocity U_s distributions at $t =$ (a) -0.17 s, (b) -0.10 s, (c) -0.03 s and (d) 0.03 s.

TSUNAMI WAVE RECORDINGS

Landslide tsunamis are generated by a rapid transfer of momentum from the landslide mass to the water body during the impact and penetration. The initial impact of the landslide with the water body transfers a portion of the landslide kinetic energy to the water body. This results in displacement of water around the impact region which moves radially outwards forming the crest of the leading wave front. The downward rush of water behind the landslide results in the formation of the trough of the leading wave front. The water displacement reaches the maximum extent when the restoring forces tend to drive the fluid back to its undisturbed state. Owing to the direction of the landslide motion and momentum transfer, the restoring forces are strongest in the lateral direction compared with the longitudinal direction. The collapse of the crater and associated uprush of water forms the crest of the second wave front. By mass conservation, the uprush is followed by a depression on the water surface which forms the trough of the second wave. Post surface restoration, the flow field consists of transient oscillations producing runup and rundown on the hill slope. This results in the formation of the trailing wave train after the first main two waves. The water displacement during the landslide impact with the water body and the tsunami wave generation is shown in Fig. 6.

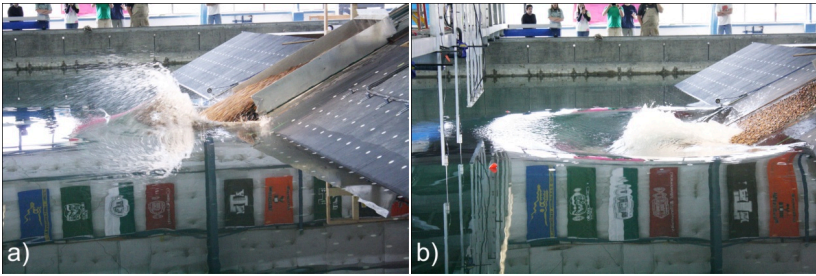


Fig. 6. (a) Water displacement during landslide impact with the water body, (b) leading radial wave propagation and trailing wave formation.

In the present experimental setup, tsunamis generated by landslides are studied in three separate setup configurations representing a fjord, headland and farfield runup. The presence of topographical and bathymetric features around the impact region and in wave propagation can either amplify or reduce the waves. The superposition of later reflected waves with the initially generated waves can lead to interference and complex wave patterns. The wave runup profiles measured on the hill slope close to the impact region for a run with landslide volume $V_s = 0.756 \text{ m}^3$, impact velocity $v_s = 5.5 \text{ m/s}$ are shown in Fig. 7 for the three setup configurations: fjords, headland; and offshore propagation and farfield runup. In the absence of any fjords or topographical structures, the wave propagates and radiates the energy away from the landslide source and the impact region. In confined topographical features, the energy is trapped and funneled between the fjord slopes. The wave reflecting from the fjord slope interferes with the generated wave train and can lead to the amplification of the wave and runup amplitudes. The onshore wave runup profiles coincide with each other until the third wave (Fig. 7a). Then the wave reflecting off the fjord slope reaches the hill slope and amplifies the wave.

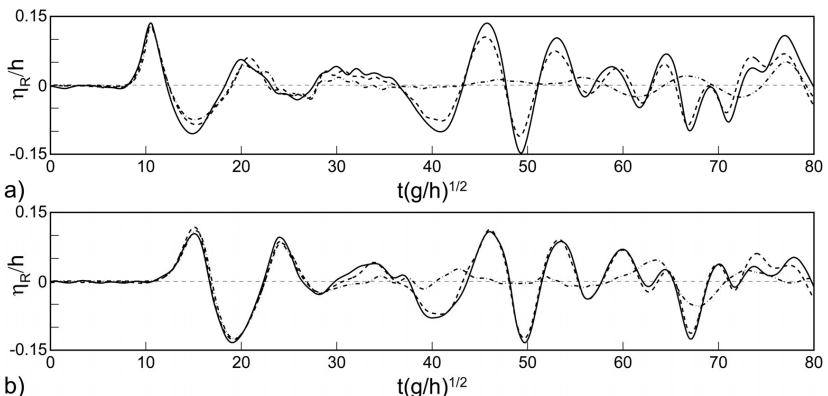


Fig. 7. Wave runup profiles measured at $r/h =$ (a) 3.3, (b) 6.3 from the impact region.
(—) fjord, (---) headland, (- · -) offshore propagation and farfield runup.

The wave profiles recorded location $(x/h, y/h) = (6.9, 0)$ m are shown in Fig. 8(a) at water depth $h = 0.6$ m. This corresponds to the wave front travelling along the direction of the landslide motion. The wave profile comparisons are shown for the case of an offshore propagating wave and effect of fjord slopes. The generated wave has a maximum amplitude in the leading wave crest with $a_c/h = 0.113$ at $t(g/h)^{0.5} = 12.82$. The trailing waves recorded on the wave gauge have altering propagating directions owing to the wave reflections from the fjord slope. In the absence of the fjord, the undisturbed wave is sustained until the sixth peak, after which wave reflections from the back and the side of the wave basin interfere with the propagating wave. In the presence of the fjord, the main reflected wave from the fjord slope reaches the propagating wave around the sixth wave as seen in the figure. The sixth crest, $a_c/h = 0.055$, $t(g/h)^{0.5} = 37.4$ corresponds to the wave reflection from the headland propagating in the opposite direction of the outward wave propagation. The corresponding peaks after the above peak correspond to the wave reflections coming from the sides of the fjord and the hill slope, which results in partial back and forth wave reflections between the fjord slopes. The corresponding wave runup profile is shown in the direction of landslide motion in Fig. 8(b).

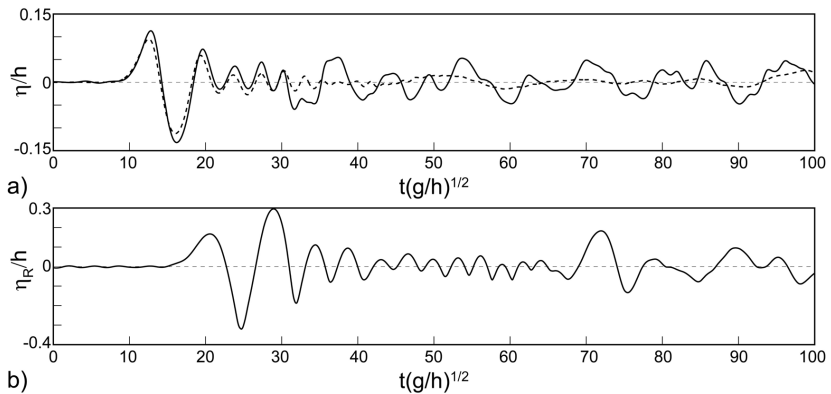


Fig. 8. (a) Wave gauge comparison between fjord (—) and farfield runup (---) case at $r/h = 6.9$, $\theta = 0^\circ$; (b) Wave runup profile on the fjord slope along the landslide direction.

The recorded wave profiles at $(x/h, y/h) = (14.1, 5.5)$ m for the same landslide parameters for the case of a headland and offshore wave propagation are shown in Fig. 9. The headland setup is similar to half of the fjord setup. A 90 degree curvature with base radius 3.26 m in the offshore slope is located in the direction of the landslide motion. The above wave gauge is located near the bend. In the absence of a headland, the generated wave has 5 wave crests after which the wave reflection from the basin walls interferes with the propagating wave. In the presence of the headland, the first two crests coincide with the undisturbed wave. The energy of the generated waves is funneled by the headland cone segment and amplifies the wave. Beyond the third wave the wave reflection from the headland slope interferes with the fourth wave which leads to the fourth peak, $a_c/h = 0.024$ at $t(g/h)^{0.5} = 44.8$ in the measured wave profile.

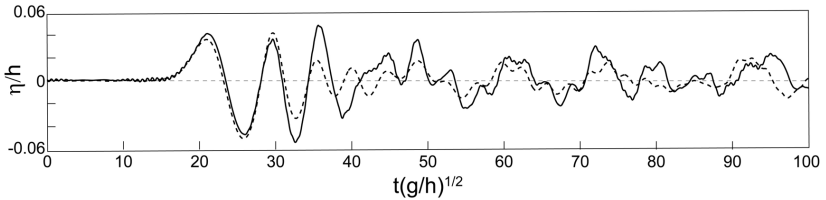


Fig. 9. Offshore wave gauge comparison between headland (—) and farfield runup (---) measured at $r/h = 15.1$, $\theta = 21.3^\circ$.

CONCLUSIONS

Tsunamis generated by granular landslides are compared in three physical model configurations representing a fjord, headland and offshore propagation and farfield runup. Measurements are made relating to the landslide shape and front velocity by an array of cameras to characterize the tsunami source. The surface velocity of the subaerial granular landslide motion is determined by particle image velocimetry analysis. An array of wave gauges in the basin measure the propagating wave profile and the wave runup on the hill slope, fjord slope, headland and farfield coastline. The fjord setup traps the wave energy between the two slopes and funnels them laterally through the fjord channel. The superposition of the initially generated and reflected waves results in multiple back and forth wave reflections between the fjord walls. The wave runup on the hill slope can be amplified due to the trapped energy by the wave reflection from the fjord or the headland slopes. In contrast with the fjord, the headland configuration traps only part of the wave energy in the channel and leaks the rest of the energy into the open basin. This results in amplification of the wave profile close to the headland curve when compared with the wave propagation in the absence of such a feature.

ACKNOWLEDGEMENTS

This research is supported by the National Science Foundation (NSF) through the grants nos. CMMI-0421090, CMMI-0936603, CMMI-0402490 and CMMI-0927178. Support by the scientific personnel and technical staff at the O. H. Hinsdale wave research laboratory, Oregon State University, Corvallis and the Network of Earthquake Engineering Simulation (NEES) are acknowledged.

REFERENCES

- Bardet, J.-P., Synolakis, C., Davis, H., Imamura, F., and Okal, E. A. (2003), Landslide tsunamis: Recent findings and research directions, *Pure Appl. Geophys.*, 160, 1793–1809.
- Bondevik, S., Løvholt, F., Harbitz, C., Mangerud, J., Dawson, A., and Svendsen, J. (2005), The Storegga slide tsunami comparing field observations with numerical solutions, *Mar. Pet. Geol.*, 22, 195–208.
- DiRisio, M., DeGirolamo, P., Bellotti, G., Panizzo, A., Aristodemo, F., Molfetta, M. G., and Petrillo, A. F. (2009), Landslide-generated tsunamis runup at the coast of

- a conical island: New physical model experiments, *J. Geophys. Res.*, 114, C01009, doi: 10.1029/2008JC004858.
- Enet, F., and Grilli, S. T. (2005), Tsunami landslide generation: Modelling and experiments, *Proc., 5th Int. on Ocean Wave Measurement and Analysis, WAVES 2005*, Madrid, Spain, IAHR, Paper No. 88.
- Enet, F., Grilli, S. T., and Asce. M. (2007), Experimental study of tsunami generation by three-dimensional rigid underwater landslides, *J. Waterway Port Coast Ocean Eng.*, 133, 442–454.
- Fine, I., Rabinovich, A., Bornhold, B., Thomson, R., and Kulikov, E. (2005), The Grand Banks landslide generated tsunami of November 18, 1929: Preliminary analysis and numerical modeling, *Mar. Geol.*, 215, 45–47.
- Fritz, H. M., Hager, W. H., and Minor, H.-E. (2001), Lituya Bay case: rockslide impact and wave run-up, *Sci. Tsunami Hazards*, 19, 3–22.
- Fritz, H., M., Hager, W. H., and Minor, H.-E. (2003a), Landslide generated impulse waves: part 1: instantaneous flow fields, *Exp. Fluids*, 35, 505–519, doi: 10.1007/s00348-003-0659-0.
- Fritz, H., M., Hager, W., H., and Minor, H.-E. (2003b), Landslide generated impulse waves: part 2: hydrodynamic impact craters, *Exp. Fluids*, 35, 520–532, doi: 10.1007/s00348-003-0660-7.
- Fritz, H., M., Hager, W., H., and Minor, H.-E. (2004), Near field characteristic of landslide generated impulse waves, *J. Waterway Port Coastal Ocean Eng.*, ASCE 130, 287–302, doi: 10.1061/(ASCE)0733-950X(2004)130:6(287).
- Fritz, H. M., Kongko, W., Moore, A., McAdoo, B., Goff, J., Harbitz, C., Uslu, B., Kalligeris, N., Suteja, D., Kalsum, K., Titov, V., Gusman, A., Latief, H., Santoso, E., Sujoko, S., Djulkarnaen, D., Sunendar, H., and Synolakis, C. (2007), Extreme runup from the 17 July 2006 Java tsunami, *Geophys Res. Lett.*, 34, L12602, doi:10.1029/2007GL029404.
- Fritz, H. M., Mohammed, F., and Yoo, J. (2009), Lituya bay landslide impact generated megatsunami 50th anniversary, *Pure Appl. Geophys.*, 166, 153–175, doi:10.1007/s00024-008-0435-4.
- Grilli, S., T., and Watts, P. (2005), Tsunami generation by submarine mass failure I: Modeling, experimental validation, and sensitivity analyses, *J. Waterway Port Coast Ocean Eng.*, 131, 283–297.
- Heinrich, P. (1992), Nonlinear Water Waves Generated by Submarine and Aerial Landslides, *J. Waterways, Port, Coastal and Ocean Eng.*, ASCE 118 (3), 249–266.
- Liu, P.-F., Wu, T.-R., Raichlen, F., Synolakis, C. E., and Borrero, J. C. (2005), Runup and rundown generated by three-dimensional sliding masses, *J. Fluid Mech.*, 536, 107–144.
- Miller, D. J. (1960), Giant waves in Lituya Bay, Alaska, Geological Survey Professional Paper, 354, C. U.S. Government Printing Office, Washington, D.C.
- Müller, L. (1964), The rock slide in the Vajont Valley, *Rock Mech. Eng. Geol.*, 2, 148–212.
- Mohammed, F., H.M. Fritz (2010). Experiments on tsunamis generated by 3D granular landslides, D.C. Mosher et al. (eds.), Submarine Mass Movements and